Exogenous Agent-Free Synthetic Post-contrast Imaging with a Cascade of Deep Networks for Enhancement Prediction After Tumor Resection

A Parametric-Map Oriented Approach

Moya-Sáez, Elisa; de Luis-García, Rodrigo; Nunez-Gonzalez, Laura; Alberola-López, Carlos; Hernández-Tamames, Juan Antonio

DOI
10.1007/978-3-031-73281-2_11

Publication date
2025

Document Version
Final published version

Published in
Simulation and Synthesis in Medical Imaging

Citation (APA)
Moya-Sáez, E., de Luis-García, R., Nunez-Gonzalez, L., Alberola-López, C., & Hernández-Tamames, J. A. (2025). Exogenous Agent-Free Synthetic Post-contrast Imaging with a Cascade of Deep Networks for Enhancement Prediction After Tumor Resection: A Parametric-Map Oriented Approach. In V. Fernandez, J. M. Wolterink, D. Wiesner, S. Remedios, L. Zuo, & A. Casamitjana (Eds.), *Simulation and Synthesis in Medical Imaging: 9th International Workshop, SASHIMI 2024, Held in Conjunction with MICCAI 2024, Marrakesh, Morocco, October 10, 2024, Proceedings* (pp. 113-123). (Lecture Notes in Computer Science; Vol. 15187 LNCS). Springer. https://doi.org/10.1007/978-3-031-73281-2_11

Exogenous Agent-Free Synthetic Post-contrast Imaging with a Cascade of Deep Networks for Enhancement Prediction After Tumor Resection. A Parametric-Map Oriented Approach

Elisa Moya-Sáez[1(✉)], Rodrigo de Luis-García[1], Laura Nunez-Gonzalez[2], Carlos Alberola-López[1], and Juan Antonio Hernández-Tamames[2,3]

[1] Laboratorio de Procesado de Imagen, Universidad de Valladolid, Valladolid, Spain
{elisa.moya,rodrigo.luis,carlos.alberola}@uva.es
[2] Radiology and Nuclear Medicine Department, Erasmus MC, Rotterdam, The Netherlands
{l.nunezgonzalez,j.hernandeztamames}@erasmusmc.nl
[3] Imaging Physics Department, TU Delft, Delft, The Netherlands

Abstract. Gadolinium-based contrast agents (GBCAs) have become a cornerstone in clinical routine for detection, characterization and monitoring of several diseases. Particularly, GBCAs are clinically relevant for the detection of blood brain barrier (BBB) damage, which is associated with an aggressive tumor behavior. However, issues such as safety concerns related to deposition of GBCA in the brain, prolonged acquisitions, and cost increase advocate against its usage. In this work, we propose a novel approach based on a cascade of deep networks for pre- and post-contrast parametric mapping and the synthesis of post-contrast T1-weighted images. Only a pair of pre-contrast weighted images acquired with conventional pulse sequences are used as inputs; thus, our approach is GBCAs-free. Results reveal the potential of this approach to obtain T1w-enhancement information after tumor resection which is comparable with another state-of-the-art prediction approach. We provide not only the predictions, but also the pre- and post-contrast parametric maps without the usage of GBCAs.

Keywords: GBCAs · Synthetic MRI · Parametric mapping · Gliomas · T1w-enhancement prediction

1 Introduction

Gadolinium-based contrast agents (GBCAs) have become a cornerstone in magnetic resonance imaging (MRI) routine for detection, characterization and monitoring of several diseases, such as multiple sclerosis [1], Alzheimer's disease [2], and brain tumors [3] among others. Indeed, 40% of all MRI acquisitions in Europe and in the United States use GBCAs [4]. Specifically, GBCAs are clinically relevant for improving lesion detection and monitoring brain tumors due to

V. Fernandez et al. (Eds.): SASHIMI 2024, LNCS 15187, pp. 113–123, 2025.
https://doi.org/10.1007/978-3-031-73281-2_11

the signal enhancement visible in the T1-weighted images after the GBCA injection, which is related with the impairment of the blood brain barrier (BBB) [5].

Although GBCAs are considered safe, 0.7–2.4% of injected patients suffer from mild adverse reactions and a lower rate from severe complications [6]. Further, the possible deposition of the GBCAs in the brain, especially in patients who have to undergo several follow-up acquisitions, has recently raised safety concerns [7]. In addition, the usage of GBCAs results in patient discomfort due to the intravenous injection, extra cost and prolonged acquisition time, being a bottleneck on daily MRI operation. Thus, making GBCAs unnecessary would be a highly desirable achievement.

In this context, parametric maps (i.e., T1, T2, and PD maps) could play a crucial role due to their quantitative nature, which makes them more robust than weighted images against scanner imperfections [8], as well as their known ability to detect subtle tumor changes. In particular, previous studies have shown that enhancing regions present different pre-contrast T1 and T2 values compared with normal white matter [9,10]. However, the acquisition of parametric maps is not widespread in the clinical practice due to the need for lengthy relaxometry acquisitions and/or scarcely available commercial sequences.

In addition, deep learning (DL) has shown remarkable results in a wide range of image processing applications, such as reconstruction, synthesis, and parametric mapping [11–13], and it constitutes a valuable tool for avoiding the usage of GBCAs in MRI exams. Recently, a growing corpus of DL works which aim at decreasing, or even eliminating, the need of GBCAs in MRI has been proposed [14–17]. These works propose methods for the synthesis of full-dose post-contrast weighted images from either low-dose or pre-contrast acquisitions, using different network architectures. However, to the best of our knowledge, these methods are focused on obtaining only post-contrast weighted images, and they leave parametric maps aside.

In this work, we propose a novel approach based on a cascade of deep networks for pre- and post-contrast parametric mapping and the synthesis of post-contrast T1-weighted (post-T1w) images. Only a pre-contrast T1-weighted (T1w) and a T2-weighted (T2w) acquired with conventional pulse sequences are used as inputs of the cascade. The performance of the synthesized weighted images for T1w-enhancement prediction after tumor resection is also evaluated and compared favourably with the state-of-the-art [9].

2 Materials and Methods

2.1 Dataset

A dataset of 15 patients with different grades of gliomas was employed in this study. All the acquisitions were performed with Institutional Review Board approval and informed written consent. Acquisitions were performed with a 3T GE Sigma Premier system (General Electric Medical Systems, Waukesha, WI 53,188 USA). All patients had undergone tumor resection before the scan.

For each patient, the imaging protocol consisted of four weighted images—T1w, T2w, T2w-FLAIR (fluid attenuation inversion recovery) and post-T1w—together with a pre-contrast MAGiC [18] acquisition for T1, T2, and PD parametric mapping. Details about sequence parameters are provided in the Appendix. In one patient the T2w-FLAIR was not acquired due to a protocol deviation.

2.2 Preprocessing

First, all image modalities were reoriented to match the orientation of the standard MNI152 template [19]. Second, all of them were skull-stripped using HD-BET [20] and linearly registered to the T1w images using FLIRT of FSL [21]. The pre-processed T1w, T2w, T2w-FLAIR, and post-T1w images were employed as input of the HD-GLIO segmentation tool [22,23], which performs tumor segmentation in two different regions: (a) contrast-enhancing tumor (T1e), and (b) non-enhancing T2w/T2w-FLAIR signal abnormality (T2h). Hereinafter, the union of these two regions is referred to as abnormal tissue (ABN). Finally, weighted images were normalized by dividing each of them by its average intensity, background excluded, prior to entering the network.

2.3 Proposed Approach: *Cascade CNNs*

The pipeline we propose (Fig. 1) consists of a cascade of two convolutional neural networks (CNNs), namely, an *extraction network* and a *prediction network*. The first network extracts the quantitative T1, T2, and PD parametric maps, whose information is embedded in the weighted images. The second network takes these T1 and T2 maps and predicts the corresponding post-contrast T1 and T2 maps (i.e., post-T1 and post-T2). Note that post-contrast refers to as the maps that would be obtained after the GBCA administration. Both networks share the same architecture described in [12] except for the number of inputs.

The training of the cascade of CNNs is performed in two steps. First, the *extraction network* is trained in a supervised way with MAGiC maps as ground-truth (step 1 in Fig. 1). The loss function used is defined as:

$$L_{\text{step1}} = ||(\text{T1}_c - \text{T1}_{gt})||_{\ell 1} + ||(\text{T2}_c - \text{T2}_{gt})||_{\ell 1} + ||(\text{PD}_c - \text{PD}_{gt})||_{\ell 1}, \quad (1)$$

where subscript c stands for *computed* and gt for *ground-truth* MAGiC maps.

Second, keeping the weights of the *extraction network* fixed, the *prediction network* is trained in a self-supervised way [24] by synthesizing weighted images from the post-contrast parametric maps (step 2 in Fig. 1). This way, we overcome the lack of post-contrast parametric maps to train the *prediction network* in a supervised way. To ensure that post-contrast maps are numerically and physically coherent, more than one weighted image should be synthesized. It is known that GBCAs reduce both T1 and T2 values of tissues, but due to the considerably longer T1 values compared to T2, their primary impact at low doses consists of T1 shortheing [5]. For this reason, T2w images can be consider

virtually invariant to contrast administration [10,25], making them the perfect candidates to guarantee the coherence of the maps. Thus, we synthesize the post-T1w and T2w images from the post-T1, post-T2 and PD maps using the following theoretical equations:

$$\text{postT1w}_{\text{syn}}(\mathbf{x}) = \text{PD}(\mathbf{x})\frac{1 - 2e^{-\frac{\text{TI}}{\text{post-T1}(\mathbf{x})}} + e^{-\frac{\text{TR}}{\text{post-T1}(\mathbf{x})}}}{1 + \cos(\alpha)e^{-\frac{\text{TR}}{\text{post-T1}(\mathbf{x})}}}\sin(\alpha)e^{-\frac{\text{TE}}{\text{post-T2}(\mathbf{x})}} \quad (2)$$

$$\text{T2w}_{\text{syn}}(\mathbf{x}) = \text{PD}(\mathbf{x})\left[1 - e^{-\frac{\text{TR}}{\text{post-T1}(\mathbf{x})}}\right]e^{-\frac{\text{TE}}{\text{post-T2}(\mathbf{x})}}, \quad (3)$$

where TE is the echo time, TR is the repetition time, TI is the inversion time and α is the flip angle.

The loss function employed for the training of the *prediction network* is intended not only to achieve visual resemblance between the synthesized and the acquired weighted images but also to capture local characteristics within the tumor. Consequently, it consists of three terms:

$$\begin{aligned} L_{\text{step2}} = &||(\text{postT1w}_{\text{syn}} - \text{postT1w}_{\text{acq}})||_{\ell 1} + ||(\text{T2w}_{\text{syn}} - \text{T2w}_{\text{acq}})||_{\ell 1} \\ &+ \lambda||M \odot (\Delta\text{T1w}_{\text{syn}} - \Delta\text{T1w}_{\text{acq}})||_{\ell 1}, \end{aligned} \quad (4)$$

where $\text{postT1w}_{\text{syn}}$ and $\text{postT1w}_{\text{acq}}$ are the synthesized and acquired post-T1w images, respectively. Similar distinction is applied to T2w_{syn} and T2w_{acq}. M is a binary mask with positive values in the T1e regions within the tumor, $\Delta\text{T1w}_{\text{syn}}$ and $\Delta\text{T1w}_{\text{acq}}$ are the GBCA intakes (i.e., $\text{postT1w}_{\text{syn}} - \text{T1w}_{\text{acq}}$ and $\text{postT1w}_{\text{acq}} - \text{T1w}_{\text{acq}}$, respectively), and $\odot$ refers to Hadamard product. Finally, λ is a trade-off parameter to balance the contribution of the local loss. We stress that the post-T1w images and the masks are only needed at the training stage.

2.4 Implementation Details

Cross-validation was carried out *via* leave-one-out. For each data split, one patient was used for testing and the remaining patients were randomly split between training (11 patients) and early-stopping validation (2 patients). Both networks share the same patient split with the exception of the patient without the T2w-FLAIR, which was additionally included in the training set for the extraction network but not for the prediction one.

Transfer learning techniques were employed in both networks. In the extraction network layers weights were initialized by training with a purely synthetic dataset [12]. In the prediction network weights were initialized by pretraining with a larger public dataset [26] of glioblastoma patients with no resection. Only the decoders were re-trained in the prediction network. Additionally, data augmentation with horizontal flips was included for the training of the prediction network. Both networks were trained with Adam optimizer (learning rate =

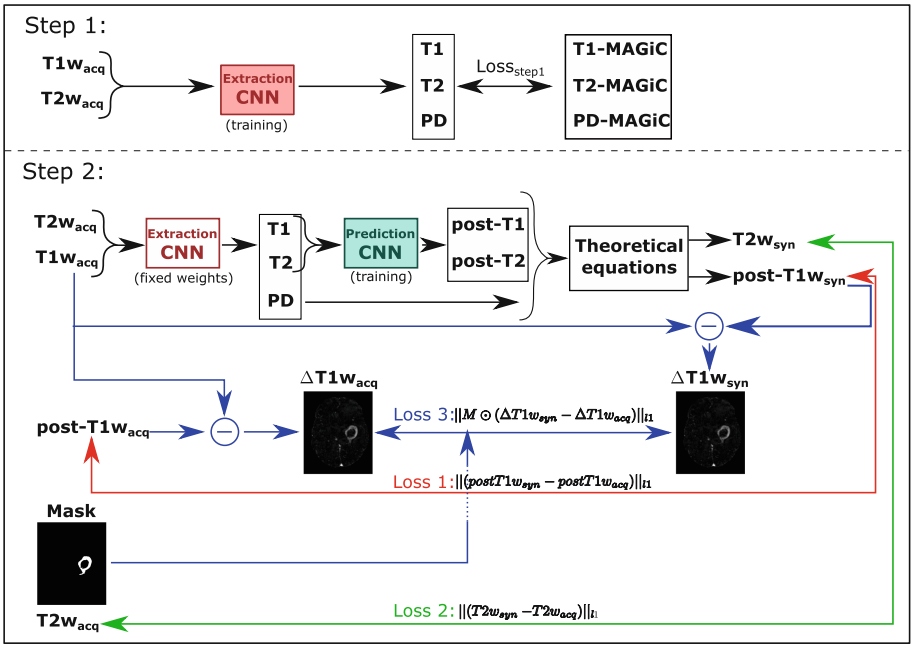

Fig. 1. Overview of the proposed approach. The cascade of CNNs is composed of an *extraction* and a *prediction network*. In step 2 only the *prediction network* is trained and the color of the arrows represents the computations related to each loss term. Loss term 1 (red arrows) focuses on achieving visual and structural resemblance between the acquired and synthesized post-T1w, loss term 2 (green arrows) ensures the obtaining of physical coherent post-contrast parametric maps values, and loss 3 (blue arrows) tries to capture local characteristics within the tumor. (Color figure online)

1e−4) and early-stopping. Batchsize of 4 (in both networks) and λ=100 were empirically set. The experiments were conducted on a GPU NVIDIA Quadro RTX 6000 with 24 GB of memory.

2.5 Evaluation

The impact that the synthesized post-T1w images could have in clinical practice should be assessed with quantitative algorithms for improving clinical decision-making.The main role of post-T1w images is assessment of the presence/absence of tumor T1w-enhancement. In what follows, the segmentations of HD-GLIO [22,23] when fed with the four acquired weighted images (i.e., pre-contrast T1w, T2w and T2w-FLAIR as well as post-T1w) is considered the ground-truth. For the validation of our method, we used the three pre-contrast acquired weighted images, as well as the synthesized post-T1w to segment T1e and T2h regions also with HD-GLIO (recall Sect. 2.2 for definitions). The results obtained were compared with another recently proposed approach for T1w-enhancement prediction without GBCAs [9]. This approach (hereafter referred to as *Voxelwise*

MAGiC) carries out a voxel-wise classification using pre-contrast maps obtained with MAGiC. In this work, *Voxelwise MAGiC* was computed with the best metric and threshold reported in [9] for classification problems C-I) ABN vs. normal tissue, and C-II) T1e vs non T1e. Note that the output of these two classifications are equivalent to the T1e and T2h segmentations reported by HD-GLIO.

Thus, our evaluation consists in comparing closeness of both our method *Cascade CNNs* and *Voxelwise MAGiC* to the ground-truth. The accuracy of both segmentations with respect to the ground-truth is separately measured voxel-wise and lesion-wise as we now describe:

Voxel-Wise Evaluation. We voxel-wise measured the sensitivity and specificity of classification problems C-I and C-II for both *Voxelwise MAGiC* and our method *Cascade CNNs*.

Lesion-Wise Evaluation. Images that show the presence of T1w-enhancement in the surroundings of the tumor area, even though the T1w-enhancement they show does not cover the whole tumor, could be valuable for decision making. To reflect this idea, we have designed a lesion-wise performance measurement consisting in: 1) the computation of clusters of voxels whose sizes are larger than 10% of the total volume of T1e in the ground-truth mask; and 2) the computation of the sensitivity considering a true positive when any of these clusters are, totally or partially, included within the ground-truth T1e segmentation. This metric is computed for both the *Voxelwise MAGiC* and our method *Cascade CNNs*.

3 Results and Discussion

Figure 2 shows the pre-contrast ground-truth maps and also the pre- and post-contrast computed maps for different test patients. Interestingly, a shortening in the post-T1 values can be noticed within the T1w-enhancement region, which is in agreement with the literature [5,10,25].

Figure 3 shows both the synthesized and the actually acquired post-T1w images for different test patients. The corresponding ground-truth and synthetic HD-GLIO segmentations are also shown overlaid on the acquired post-T1w and synthesized post-T1w, respectively. Note that the post-T1w images are synthesized from the computed post-contrast parametric maps shown in Fig. 2. The synthesized post-T1w images can be visually compared with their actually acquired counterparts and visual resemblance is noticeable.

Results of voxel-wise and lesion-wise evaluations are shown in Tables 1 and 2, respectively. Table 1 shows a superiority of *Voxelwise MAGiC* in terms of sensitivity, although lower specificity values are reported with this method. As for our method, we have observed that the enhanced areas in the synthesized images do not show a by-point coincidence with ground-truth despite these images indeed show the presence of T1w-enhancement, as required by clinical practice. This fact can be appraised in the metrics of Table 2 where *Cascade CNN* achieves

comparable performance with *Voxelwise MAGIC*. *Cascade CNN*, in addition, provides the post-contrast parametric maps as a byproduct.

This work also presents some limitations. Computed maps show some blurring, especially in the interfaces between tissues. This fact may be caused by misregistrations of the input weighted images. Additionally, the comparison of the computed post-contrast parametric maps with those obtained with other well-accepted techniques should be performed for a thorough validation. In addition, a validation with a larger cohort is desirable.

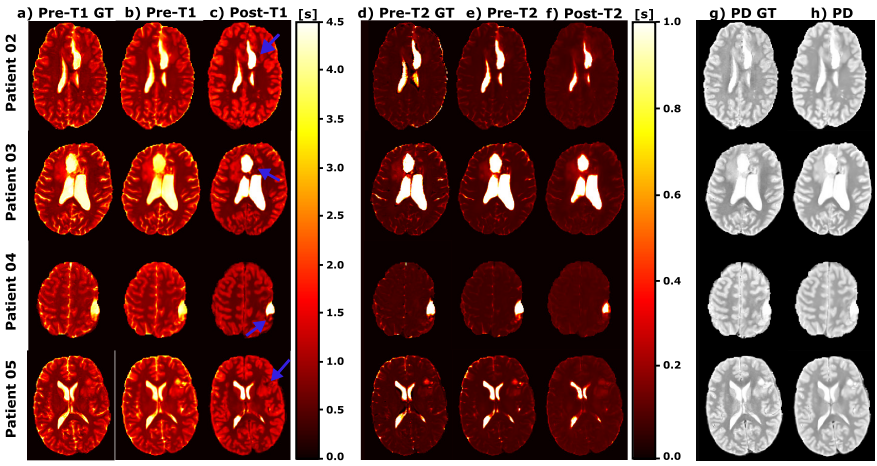

Fig. 2. A representative axial slice of the pre- and post-contrast parametric maps on different test patients. a) Pre-contrast T1 ground-truth maps. b) Pre-contrast T1 computed maps. c) Post-contrast T1 computed maps. d) Pre-contrast T2 ground-truth maps. e) Pre-contrast T2 computed maps. f) Post-contrast T2 computed maps. g) PD ground-truth maps. h) PD computed maps. T1 and T2 values are measured in seconds [s]. Blue arrows indicates the shortening in the post-T1 values within the T1w-enhancement region. Note that PD is not affected by the GBCA. (Color figure online)

Table 1. Sensitivity and specificity of the voxel-wise predictions for both classification problems (i.e., C-I) ABN vs. Normal Tissue and C-II) T1e vs. non T1e) and both methods—*Voxelwise MAGIC* and *Cascade CNNs* —.

Method	C-I) ABN vs. Normal Tissue		C-II) T1e vs. non T1e	
	Sensitivity	Specificity	Sensitivity	Specificity
Voxelwise MAGIC	89.35%	93.61%	87.29%	94.95%
Cascade CNNs	77.92%	99.95%	50.20%	99.40%

Table 2. Sensitivity of the lesion-wise T1w-enhancement prediction for each patient and both methods. Note that only the patients with T1w-enhancing lesions are considered. Bold text represents the superiority of the *Cascade CNN* method, whereas inferiority is represented with underlined text.

Patient ID	00	01	02	03	04	05	07	08	09	12	13
Voxelwise MAGiC	33%	40%	100%	100%	75%	33%	100%	100%	100%	100%	50%
Cascade CNN	**100%**	**50%**	100%	50%	50%	**100%**	100%	100%	100%	100%	0%

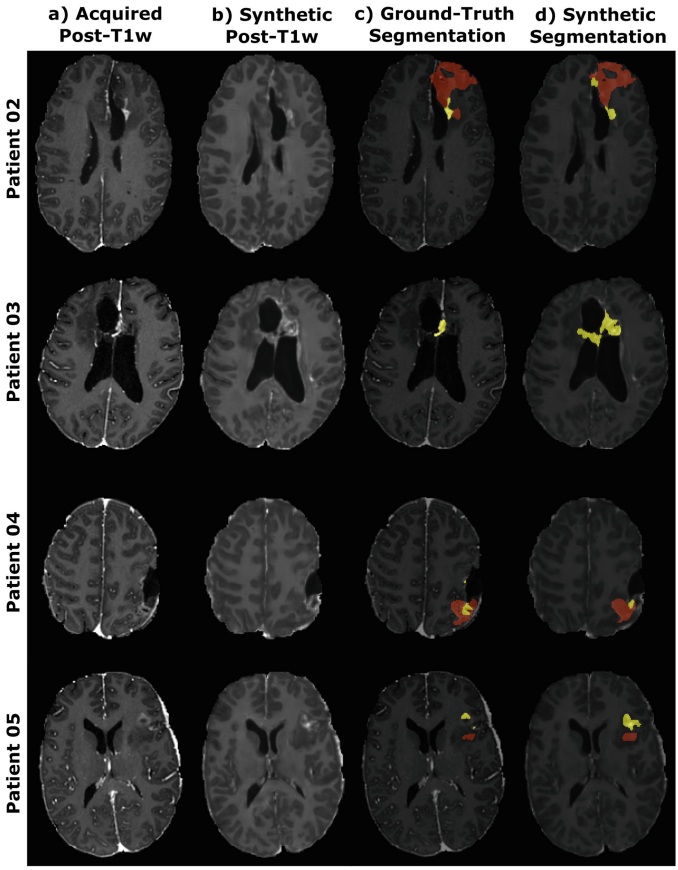

Fig. 3. A representative axial slice of the synthesized post-T1w images for different test patients. a) Acquired post-T1w. b) Synthesized post-T1w. c) Ground-truth segmentation masks of HD-GLIO. d) Corresponding segmentation masks of HD-GLIO using the synthesized post-T1w instead of the acquired one. Red label represents T2h, whereas the yellow label represents T1e. (Color figure online)

4 Conclusion

A novel approach for pre- and post-contrast parametric mapping and the synthesis of post-contrast T1w images is proposed. The computation is based on a cascade of CNNs and only needs a pair of pre-contrast conventional weighted image as input; these images turn out to be those customarily used in clinical practice. Our results suggest the potential of this approach for replacing GBCAs in T1w-enhancement assessment.

Acknowledgments. This work was supported by the Asociación Española Contra el Cáncer, the Ministerio de Ciencia e Innovación of Spain (grants PID2020-115339RB-I00, TED2021-130090B-I00, and PID2021-124407NB-I00), the General Electric Healthcare (grant "B-GEHC-5. MR Physiological Signature"), and ESAOTE. The authors also acknowledge the funding from "la Caixa" Foundation and FCT, I.P. (grant number LCF/PR/HR22/00533).

Appendix

Table 3 includes the sequence parameters used for the acquisition of the different image modalities, namely, T1w, T2w, T2w-FLAIR, post-T1w, and pre-contrast MAGiC for T1, T2 and PD parametric mapping.

Table 3. Details about the sequence parameters used for the acquisition of the different image modalities. These parameters are field-of-view (FOV), echo time (TE), repetition time (TR), inversion time (TI), and flip angle (α).

Scan parameters	T1w	T2w	T2w-FLAIR	post-T1w	MAGiC
Acquisition type	3D	2D	3D	3D	2D
Plane	Axial	Axial	Sagittal	Axial	Axial
Voxel size	1.0×1.0 mm	0.6×0.6 mm	1.1×1.1 mm	1.0×1.0 mm	1.0x1.0 mm
Slice Thickness	1.0 mm	3.0 mm	1.6 mm	1.0 mm	3.0 mm
Slice Spacing	-	3.0 mm	-	-	3.0 mm
# Slices	352	49	224	352	49
FOV	240×240 mm	233×233 mm	246×246 mm	240×240 mm	240×240 mm
TE	3.3 ms	97 ms	89 ms	3.3 ms	6114 ms
TR	7.9 ms	9837ms	5000 ms	7.9 ms	15.7 ms
TI	450 ms	-	1588 ms	450 ms	11 ms
α	12°	90°	90°	12°	90°

References

1. Silver, N., Good, C., Barker, G., MacManus, D., Thompson, A., Moseley, I., et al.: Sensitivity of contrast enhanced MRI in multiple sclerosis. Effects of gadolinium dose, magnetization transfer contrast and delayed imaging. Brain J. Neurol. **120**(7), 1149–1161 (1997)
2. Khan, U. A., Liu, L., Provenzano, F. A., Berman, D. E., Profaci, C. P., Sloan, R., et al.: Molecular drivers and cortical spread of lateral entorhinal cortex dysfunction in preclinical Alzheimer's disease. Nature neuroscience **17**(2), 304–311 (2014).
3. Zahra, M. A., Hollingsworth, K. G., Sala, E., Lomas, D. J., Tan, L. T.: Dynamic contrast-enhanced MRI as a predictor of tumour response to radiotherapy. The lancet Oncology **8**(1), 63–74 (2007).
4. Runge, V. M.: Safety of the gadolinium-based contrast agents for magnetic resonance imaging, focusing in part on their accumulation in the brain and especially the dentate nucleus. Investigative radiology **51**(5), 273–279 (2016).
5. Warntjes, M., Blystad, I., Tisell, A., Larsson, E.-M.: Synthesizing a contrast-enhancement map in patients with high-grade gliomas based on a postcontrast MR imaging quantification only. American Journal of Neuroradiology **39**(12), 2194–2199 (2018).
6. Forghani, R.: Adverse effects of gadolinium-based contrast agents: changes in practice patterns. Topics in Magnetic Resonance Imaging **25**(4), 163–169 (2016).
7. Gulani, V., Calamante, F., Shellock, F. G., Kanal, E., Reeder, S. B.: Gadolinium deposition in the brain: summary of evidence and recommendations. The Lancet Neurology **16**(7), 564–570 (2017).
8. Weiskopf, N., Suckling, J., Williams, G., Correia, M. M., Inkster, B., Tait, R., et al. Quantitative multi-parameter mapping of R1, PD*, MT, and R2* at 3T: a multi-center validation. Frontiers in neuroscience, **7**, 95 (2013).
9. Nunez-Gonzalez, L., van Garderen, K. A., Smits, M., Jaspers, J., Romero, A. M., Poot, D. H., Hernandez-Tamames, J. A.: Pre-contrast MAGiC in treated gliomas: a pilot study of quantitative MRI. Scientific Reports **12**(1), 21820 (2022).
10. Hattingen, E., Müller, A., Jurcoane, A., Mädler, B., Ditter, P., Schild, H., et al. Value of quantitative magnetic resonance imaging T1-relaxometry in predicting contrast-enhancement in glioblastoma patients. Oncotarget **8**(32), 53542 (2017).
11. Yang, G., Yu, S., Dong, H., Slabaugh, G., Dragotti, P. L., Ye, X. et al.: DAGAN: deep de-aliasing generative adversarial networks for fast compressed sensing MRI reconstruction. IEEE transactions on medical imaging, **37**(6), 1310–1321 (2017).
12. Moya-Sáez, E., Peña-Nogales, Ó., de Luis-García, R., Alberola-López, C.: A deep learning approach for synthetic MRI based on two routine sequences and training with synthetic data. Computer Methods and Programs in Biomedicine **210**, 106371 (2021).
13. Didenko, S.V., Warfield, S., Kurugol, S., Afacan, O.: SynthMap: a generative model for synthesis of 3D datasets for quantitative MRI parameter mapping of myelin water fraction. In: 5th International Conference on Medical Imaging with Deep Learning. PMLR, vol. 172, pp. 1268–1284 (2022)
14. Gong, E., Pauly, J. M., Wintermark, M., Zaharchuk, G.: Deep learning enables reduced gadolinium dose for contrast-enhanced brain MRI. Journal of magnetic resonance imaging **48**(2), 330-340 (2018).
15. Kleesiek, J., Morshuis, J. N., Isensee, F., Deike-Hofmann, K., Paech, D., Kickingereder, P., et al.: Can virtual contrast enhancement in brain MRI replace gadolinium?: a feasibility study. Investigative radiology, **54**(10), 653–660 (2019)

16. Preetha, C. J., Meredig, H., Brugnara, G., Mahmutoglu, M. A., Foltyn, M., Isensee, F., et al. : Deep-learning-based synthesis of post-contrast T1-weighted MRI for tumour response assessment in neuro-oncology: a multicentre, retrospective cohort study. The Lancet Digital Health, **3**(12), e784–e794 (2021).
17. Moya-Sáez, E., de Luis-García, R. and Alberola-López, C.: Toward deep learning replacement of gadolinium in neuro-oncology: A review of contrast-enhanced synthetic MRI. Frontiers in Neuroimaging **2** 1055463 (2023)
18. Warntjes, J. B. M., Leinhard, O. D., West, J., Lundberg, P.: Rapid magnetic resonance quantification on the brain: optimization for clinical usage. Magnetic Resonance in Medicine **60**(2), 320–329 (2008).
19. Evans, A. C., Janke, A. L., Collins, D. L., Baillet, S.: Brain templates and atlases. Neuroimage **62**(2), 911–922 (2012).
20. Isensee F, Schell M, Tursunova I, Brugnara G, Bonekamp D, Neuberger U, et al.: Automated brain extraction of multi-sequence MRI using artificial neural networks. Human Brain Mapping **40** 4952–4964.(2019).
21. Jenkinson, M., Beckmann, C. F., Behrens, T. E., Woolrich, M. W., Smith, S. M.: Fsl. Neuroimage **62**(2), 782–790 (2012).
22. Kickingereder P, Isensee F, Tursunova I, Petersen J, Neuberger U, Bonekamp D, et al.: Automated quantitative tumour response assessment of MRI in neuro-oncology with artificial neural networks: a multicentre, retrospective study. Lancet Oncology 20(5) 728–740 (2019).
23. Isensee, F., Petersen, J., Kohl, S.A., Jäger, P.F., Maier-Hein, K.H.: nnU-Net: breaking the spell on successful medical image segmentation. arXiv preprint arXiv:1904.08128 **1**(1–8), 2 (2019)
24. Moya-Sáez, E., de Luis-García, R., Alberola-López, C.: A self-supervised deep learning approach to synthesize weighted images and T1, T2, and PD parametric maps based on MR physics priors. In: Proceedings of the ISMRM & SMRT Annual Meeting & Exhibition, 2169 (2021)
25. Lescher, S., Jurcoane, A., Veit, A., Bähr, O., Deichmann, R., Hattingen, E.: Quantitative T1 and T2 mapping in recurrent glioblastomas under bevacizumab: earlier detection of tumor progression compared to conventional MRI. Neuroradiology **57**, 11–20 (2015).
26. Bakas, S., Sako, C., Akbari, H., Bilello, M., Sotiras, A., Shukla, G., et al.: The University of Pennsylvania glioblastoma (UPenn-GBM) cohort: advanced MRI, clinical, genomics, & radiomics. Sci. Data **9**(1), 453 (2022)